ACS APPLIED MATERIALS & INTERFACES

Research Article

www.acsami.org

Numerical Characterization of Magnetically Aligned Multiwalled Carbon Nanotube–Fe_3O_4 Nanoparticle Complex

Xiaolong Jia,[†,‡] Wusheng Li,[†] Xianjuan Xu,[†] Wenbin Li,[†] Qing Cai,*[,†] and Xiaoping Yang[†,‡]

[†]State Key Laboratory of Organic–Inorganic Composites, College of Materials Science and Engineering, Beijing University of Chemical Technology, Beijing 100029, P. R. China

[‡]Changzhou Institute of Advanced Materials, Beijing University of Chemical Technology, Jiangsu 213164, P. R. China

ABSTRACT: Alignment states of one-dimensional multiwalled carbon nanotubes containing various contents of zero-dimensional ferriferrous oxide nanoparticles (MWCNT–Fe_3O_4) were numerically characterized. MWCNT–Fe_3O_4 complexes were successfully prepared via in situ surface-initiated atom transfer radical polymerization, followed by a coprecipitation process. The complexes showed strong magnetism, which endowed them with the ability to be aligned under the action of an external magnetic field. The intensity of the magnetic field, loading content of Fe_3O_4 nanoparticles, and viscosity of dispersing medium, however, all had substantial effects on the alignment degree. To evaluate the alignment effectively and quantitatively, an orientation tensor description based on marking the direction of a single MWCNT in a selected region of optical images was employed. The results showed that MWCNT–Fe_3O_4 complex containing 26 wt % of Fe_3O_4 nanoparticles achieved a desirable alignment in deionized water under a magnetic field intensity of 0.10 T. Accordingly, epoxy composites reinforced with such aligned MWCNT–Fe_3O_4 complexes displayed 12.3 and 10.9% enhancement in tensile strength and modulus, as well as 8.9 and 6.1% enhancement in flexural strength and modulus, respectively.

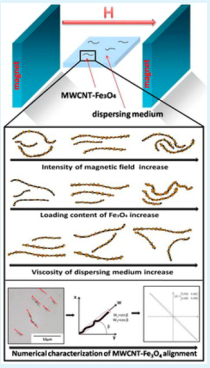

KEYWORDS: *numerical characterization, alignment, orientation tensor, multiwalled carbon nanotube, Fe_3O_4 nanoparticle*

1. INTRODUCTION

Carbon nanotubes (CNTs) have been the focus of intense research and widely applied in many fields, such as composites and biotechnology, due to their unique structure-dependent mechanical, electrical, and optical properties.[1] Specifically, the use of aligned CNTs in a variety of matrices has been developed, which could endow the resulting nanocomposites with attractive performances and anisotropic properties.[2] For instance, the lateral mechanical performance of fiber-reinforced composites could be substantially enhanced with aligned CNTs; in addition, the aligned CNTs could also be used to regulate the electrical and optical anisotropy of photoelectric composites.[3−5] However, the alignment of CNTs in polymeric matrixes was difficult to obtain, which had greatly limited their efficiency in applications.[6−8] Therefore, in preparing CNT-containing composites, the main challenge in taking full advantage of the intrinsic high performance of CNTs was how to effectively control the alignment of CNTs in matrixes.

Several methods, including flow field,[9,10] magnetic field,[11,12] and electrospinning field,[13,14] have be employed to achieve the alignment of CNTs in matrixes. Among them, the magnetic field was proven to be an effective way that the alignment of CNTs could be facilely obtained and adjusted when CNTs were functionalized with magnetic inorganic nanoparticles.[15−20] For instance, Kim et al. tethered magnetic nanoparticles onto the walls of multiwalled CNTs (MWCNTs) by means of a sol–gel process using an iron salt as precursor.[21] The resulting magnetic MWCNTs were aligned in epoxy matrix by application of an external magnetic field. Correa-Duarte et al. reported the alignment of MWCNTs in an external magnetic field through the deposition of uniform layers of magnetite/maghemite nanoparticles onto MWCNTs by combining the polymer wrapping and layer-by-layer assembly techniques.[22,23] Objectively speaking, the reported preparation process of magnetic CNTs demonstrated difficulties in controlling the synthetic conditions systematically and in adjusting the loading contents of magnetic nanoparticles quantitatively. Besides, numerical evaluation on the alignment of CNTs was lack in the literature, which obviously increased the difficulty and the uncertainty in tailoring the alignment of CNTs in matrixes. Establishing a numerical correlation between the alignment degree of CNTs and relevant affecting factors such as loading content of magnetic nanoparticles, therefore, would be very helpful in quantitatively regulating the alignment of CNTs in applications.

Herein, a facile approach was proposed to prepare magnetic MWCNTs composed of MWCNTs and ferriferrous oxide nanoparticles (MWCNT–Fe_3O_4). As schematically shown in Figure 1a, MWCNTs were first surface-grafted with polyglycidyl methacrylate (PGMA) via in situ surface-initiated atom transfer radical polymerization (ATRP) and then loaded with ferromagnetic Fe_3O_4 nanoparticles via a coprecipitation process. MWCNT–Fe_3O_4 complexes with different amounts of Fe_3O_4 nanoparticles were prepared and their tendencies in magnetic field alignment were investigated by choosing different magnetic field intensities and different dispersing

Received: October 31, 2014
Accepted: January 19, 2015
Published: January 19, 2015

DOI: 10.1021/am507583r
ACS Appl. Mater. Interfaces 2015, 7, 3170–3179

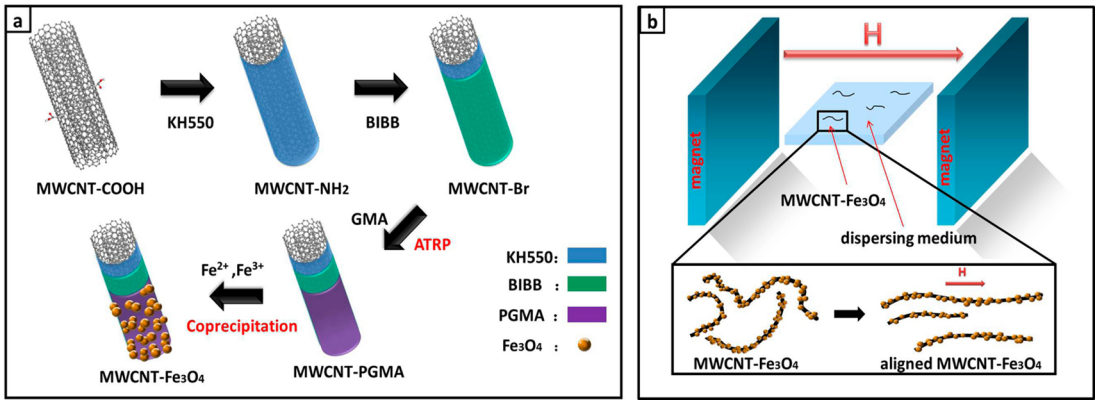

Figure 1. Schematic of (a) the MWCNT−Fe_3O_4 preparation procedure and (b) the alignment process of MWCNT−Fe_3O_4 in an external magnetic field.

Table 1. MWCNT− Fe_3O_4 Complexes Prepared and Used in the Present Study

	feeding dose			
sample	MWCNT−PGMA (g)	TMAOH (mL)	$FeCl_3{\cdot}6H_2O$ (g)	$FeCl_2{\cdot}4H_2O$ (g)
MWCNT−Fe_3O_4-1	0.10	4.40	0.220	0.100
MWCNT−Fe_3O_4-2	0.10	2.20	0.110	0.050
MWCNT−Fe_3O_4-3	0.10	1.10	0.055	0.025

medium (Figure 1b). Alignment degrees of MWCNT−Fe_3O_4 in different situations were numerically characterized using an orientation tensor description, which could be calculated from labeled morphologies of MWCNT−Fe_3O_4 using optical microscope (OM) images. Alignment mechanisms of MWCNT−Fe_3O_4 were then proposed in reference to the affecting factors. Finally, the possibility of using aligned MWCNT−Fe_3O_4 complexes as reinforcements for epoxy composites was investigated by evaluating tensile and flexural properties.

2. EXPERIMENTAL SECTION

2.1. Materials. Carboxylated MWCNTs (MWCNT−COOH; purity ≥95%, diameter 50−80 nm, length 10−20 μm) were purchased from Chengdu Organic Chemicals Co. Ltd. Glycidyl methacrylate monomer (GMA) (purity ≥97%) and 2-bromo-2-methylpropionyl bromide (BIBB) were obtained from Sigma-Aldrich Co. Silane coupling agent, KH550 (purity ≥98%), and cuprous bromide (CuBr) were obtained from Alfa-Aesar Co. *N,N,N′,N″,N″*-Pentmethyldiethylenetriamine (PMDETA) was obtained from TCI Shanghai Co. Ltd. Triethylamine was obtained from Beijing Tong Guang Fine Chemical Co. Iron salts ($FeCl_3{\cdot}6H_2O$ and $FeCl_2{\cdot}4H_2O$) were obtained from Tianjin Fuchen Chemical Reagents Factory. Tetramethylammonium hydroxide (TMAOH; purity ~25%) was obtained from Tianjin Guangfu Fine Chemical Research Institute. Tetrahydrophthalic acid diglycidyl ester type epoxy resin was supplied by Tianjin Jindong Chemical Plant. All other chemicals and reagents were purchased from Beijing Chemical Works and used directly.

2.2. Preparation of MWCNT−Fe_3O_4 Complexes. The preparation procedure of MWCNT−Fe_3O_4 complexes is shown in Figure 1a. MWCNT−COOH was strictly purified by washing with deionized water repeatedly to remove any possible impurities before use. MWCNT−NH_2 were prepared by mixing KH550 with MWCNT−COOH suspension under bath sonication as per our previous works.[24−26] The dried MWCNT−NH_2 was dispersed in tetrahydrofuran (THF) and triethylamine by bath sonication for 0.5 h, followed by the addition of BIBB/THF solution. Subsequently, the mixture was slowly stirred and allowed to react for 24 h at 30 °C. The BIBB-grafted MWCNTs (MWCNT−Br) were obtained by centrifugation, washing with absolute THF several times, and drying in vacuum. MWCNT−Br was dispersed in *N,N*-dimethylformamide (DMF) by bath sonication for 0.5 h under nitrogen and then mixed with GMA, PMDETA, and CuBr. The resulting solution was further stirred for 24 h at 30 °C. MWCNT−PGMA was obtained by centrifugation, washing with absolute ethyl alcohol several times, and drying in vacuum. The MWCNT−PGMA was redispersed in a mixture of deionized water and TMAOH by bath sonication for 1 h under nitrogen, followed by dropwise addition of Fe^{2+}/Fe^{3+} aqueous solution until the pH of the system was in the range of 11−13.[27] The final product, MWCNT−Fe_3O_4 complex, was obtained by centrifugation, washing with deionized water several times, and drying in vacuum. The prepared samples and their initial feeding doses are listed in Table 1.

2.3. Alignment of MWCNT−Fe_3O_4 Complexes. The alignment of MWCNT−Fe_3O_4 complexes in dispersing medium was conducted by a pair of magnets, as illustrated in Figure 1b. Three dispersing media, including deionized water, isobutyl alcohol, and ethylene glycol, were used to investigate the effects of their viscosities on the alignment of MWCNT−Fe_3O_4 complexes, and three magnetic field intensities (0.08, 0.10, and 0.12 T) were applied.

2.4. Composite Preparation. MWCNT−Fe_3O_4 complexes were uniformly dispersed in epoxy diluter to form the master batch. Then, epoxy mixtures were obtained by uniformly mixing epoxy resin, MWCNT−Fe_3O_4-containing master batch, and other agents in reference to our previous works.[24,28] The epoxy composites with MWCNT−Fe_3O_4 were prepared by pouring the epoxy mixture into a mold and curing at two stages. The curing process of the composites was carried out at 50 °C/5 h by applying the magnetic field along the length direction of composite sample, followed by continuously curing at 80 °C/1 h + 100 °C/1 h + 120 °C/3 h after removing the magnetic field. The pristine epoxy and epoxy composites containing MWCNT−Fe_3O_4 were also prepared by using the same process as references in absence of magnetic field. The content of MWCNT−Fe_3O_4 was fixed at 0.5 wt % of resin matrix.

2.5. Characterizations. Changes of the functional groups on the surface of MWCNTs were detected with Fourier transform infrared spectroscopy (FT-IR, Nexus670, Nicolet). Loading contents of Fe_3O_4 nanoparticles onto MWCNTs were measured on thermogravimetric analyzer (TGA, Q500, TA) at a heating rate of 10 °C/min from 50 to 600 °C under a nitrogen atmosphere. Morphologies of functionalized MWCNTs were observed by both scanning electron microscope (SEM, S4700, Hitachi) and transmission electron microscope (TEM,

DOI: 10.1021/am507583r
ACS Appl. Mater. Interfaces 2015, 7, 3170−3179

JEM100CX, Leica). Average sizes of Fe_3O_4 nanoparticles were obtained by measuring at least 200 particles using ImageJ software (National Institutes of Health, USA) and SEM images. The crystal structure of Fe_3O_4 nanoparticles was investigated by a high-resolution transmission electron microscope (HR-TEM, H-800, Hitachi). The magnetic properties of MWCNT−Fe_3O_4 complexes were investigated by vibrating sample magnetometer (Lake Shore 7410 VSM). The morphology and the alignment of as-prepared samples were characterized using SEM and optical microscope (IX51-21PH). Tensile and flexural properties of epoxy composites were measured by a mechanical testing machine (INSTRON 1121) according to ASTM D 638 and ASTM D 790, respectively. All final values of tensile and flexural properties were averages of five measurements.

3. RESULTS AND DISCUSSION

3.1. Characterization of MWCNT−Fe_3O_4 Complex.

Figure 2 shows FT-IR spectra of functionalized MWCNTs at different preparation stages. Compared to the original MWCNT−COOH, an additional peak at 1129 cm^{-1} in the spectrum of MWCNT−NH_2 corresponded to the bending vibration of Si−O−C_2H_5. Together with the presence of characteristic peaks of the Si−C group at 830 cm^{-1} and the −NH_2 group at 1558 cm^{-1}, the successful grafting of coupling agent KH550 onto MWCNTs could be confirmed. In the spectrum of MWCNT−Br, the absorption peak at 630 cm^{-1} was attributed to the introduction of the C−Br group, indicating the occurrence of bromization. After surface-initiated polymerization of GMA, the FT-IR spectrum of the resulting MWCNT−PGMA clearly displayed characteristic adsorptions of C═O stretching vibrations at 1633 and 1721 cm^{-1}, which apparently came from carboxylic groups and ester groups contained in the GMA component, respectively. Additionally, two adsorption peaks at 1125 and 1248 cm^{-1} originated from the asymmetrical and symmetrical stretching peak of the −CH_3 group in GMA units, respectively, and the absorption peak at 902 cm^{-1} was ascribed to epoxide groups in GMA units.[29] In the three cases of MWCNT−Fe_3O_4 complexes, a sharp and strong peak at 1384 cm^{-1} was detected. It resulted from the stretching vibration of Fe−O−Fe bonds,[30] which manifested the abundant existence of iron oxides in MWCNT−Fe_3O_4 complexes.

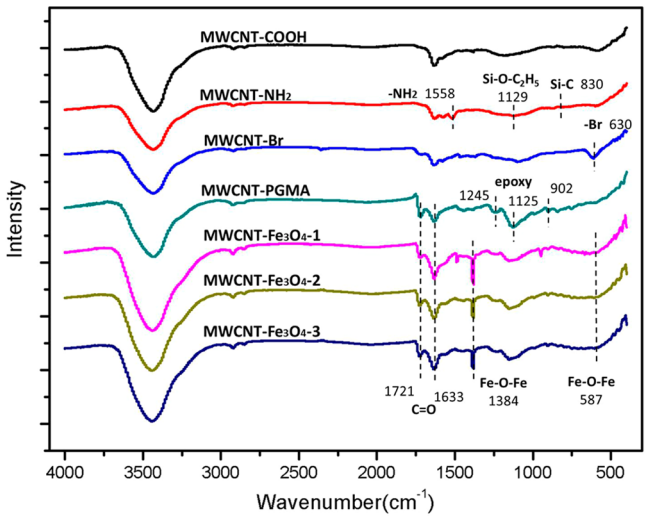

Figure 2. FT-IR spectra of MWCNT−COOH, MWCNT−NH_2, MWCNT−Br, MWCNT−PGMA, and MWCNT−Fe_3O_4 complexes.

Figure 3 shows TGA curves of functionalized MWCNTs at different preparation stages. Compared with the value of 0.9 wt % for MWCNT−COOH, the weight loss at 600 °C increased gradually in values of 2.2, 2.6, and 32.1 wt % for MWCNT−NH_2, MWCNT−Br, and MWCNT−PGMA, respectively, indicating the success in each step of synthesis.[15,31,32] The weight losses of MWCNT−Fe_3O_4 complexes, however, decreased in comparison with that of MWCNT−PGMA. The values were 21.5, 23.7, and 29.6 wt % for MWCNT−Fe_3O_4-1, MWCNT−Fe_3O_4-2, and MWCNT−Fe_3O_4-3, respectively. The phenomena resulted from the incorporation of iron oxides onto MWCNTs, because iron oxides were stable at 600 °C in nitrogen atmosphere.[33] Noticeably, the weight losses for MWCNT−Fe_3O_4-1, MWCNT−Fe_3O_4-2, and MWCNT−Fe_3O_4-3 distinctively increased in turn, proving that the loading content of iron oxides onto MWCNTs was well-controlled by decreasing the content of iron ions in the solution during the coprecipitation process (Table 1). The weight content of iron oxides on MWCNTs could be thus calculated using the equation $f_{MWCNT-Fe_3O_4} = (1 - X)f_{MWCNT-PGMA}$,[34] where $f_{MWCNT-Fe_3O_4}$ and $f_{MWCNT-PGMA}$ are the percentage of the weight loss of MWCNT−Fe_3O_4 and MWCNT−PGMA, respectively, and X denotes the weight content of iron oxides in MWCNT−Fe_3O_4 complex. The calculated weight contents of iron oxides in MWCNT−Fe_3O_4-1, MWCNT−Fe_3O_4-2, and MWCNT−Fe_3O_4-3 were 33, 26, and 8 wt %, respectively.

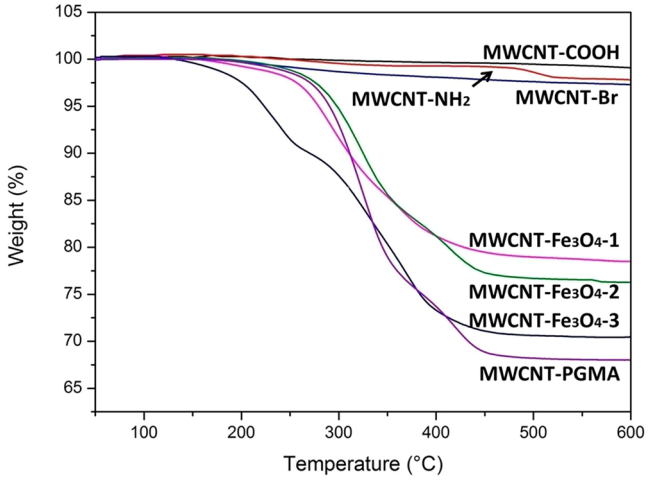

Figure 3. TGA curves of MWCNT−COOH, MWCNT−NH_2, MWCNT−Br, MWCNT−PGMA, and MWCNT−Fe_3O_4 complexes.

Morphologies of MWCNT−COOH, MWCNT−PGMA, and MWCNT−Fe_3O_4-2 were observed by both SEM and TEM. The typical hollow, rodlike structure with smooth surface was observed for MWCNT−COOH (Figure $4a_1,a_2$), while MWCNT−PGMA looked very rough and distinctively showed an 8 nm coating shell from the wrapped edge (Figure $4b_1,b_2$), confirming the successful grafting of PGMA onto MWCNT. This observation was similar to the result in the literature.[35] For MWCNT−Fe_3O_4-2, the mass of the nanoparticles with an average diameter of 25.5 nm was found uniformly distributing on the surface of the MWCNT (Figure $4c_1,c_2,d_1$), which indicated the deposition of iron oxide nanoparticles onto MWCNTs. The HRTEM image and the inset image in Figure $4d_2$ illustrate the featured lattice structure and characteristic electron diffraction patterns of Fe_3O_4 nanoparticles with high

DOI: 10.1021/am507583r
ACS Appl. Mater. Interfaces 2015, 7, 3170−3179

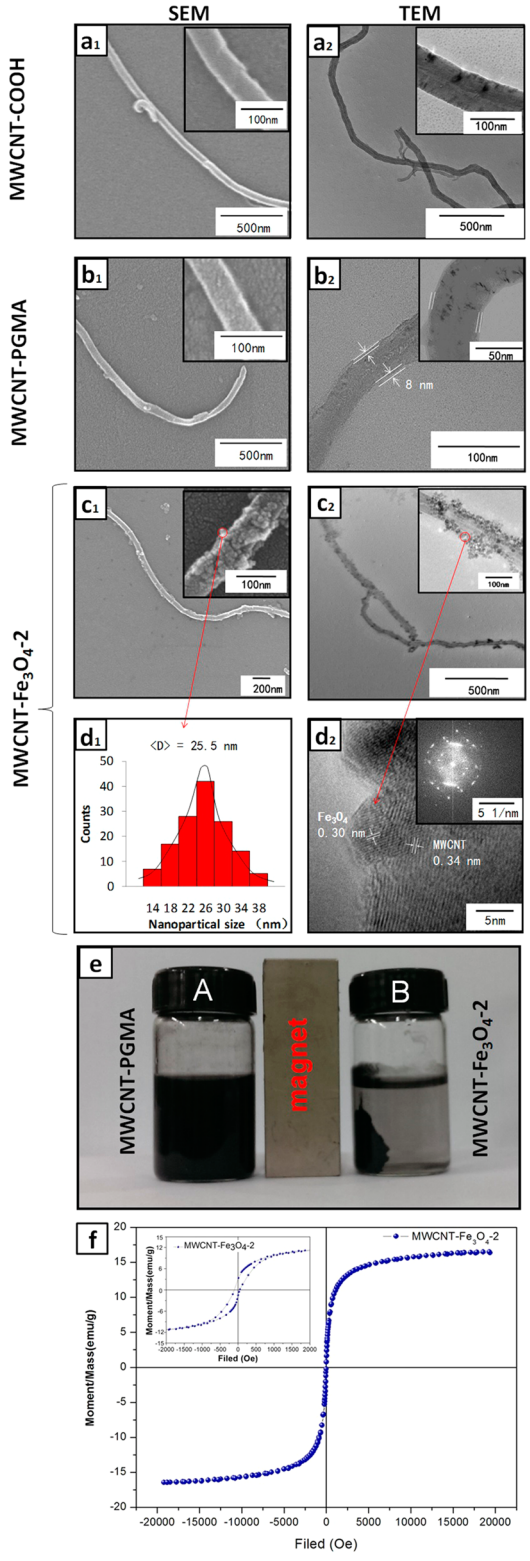

Figure 4. (a_1, b_1, c_1) SEM and (a_2, b_2, c_2) TEM images of MWCNT−COOH, MWCNT−PGMA, and MWCNT−Fe_3O_4-2, together with (d_1) size distribution of Fe_3O_4 nanoparticles, (d_2) HR-TEM image and (inset) electron diffraction patterns of Fe_3O_4 nanoparticles, (e) optical images of MWCNT−PGMA (labeled as A) and MWCNT−Fe_3O_4-2 (labeled as B) in deionized water next to a magnet, and (f) magnetic hysteresis loops for MWCNT−Fe_3O_4-2 obtained at 298 K. The insets in panels of a_1, a_2, b_1, b_2, c_1, c_2, and f are the corresponding high-magnification images.

crystallinity.[20] The interlayer spacing of the (220) lattice plane of Fe_3O_4 nanoparticles was measured to be 0.30 nm, and the interlayer spacing of MWCNT was 0.34 nm, which agreed with the results in the literature.[36,37] Furthermore, the magnetic nature of as-prepared MWCNT−Fe_3O_4 was easily evaluated by placing an external magnet next to the vials containing the aqueous solution of MWCNT−PGMA or MWCNT−Fe_3O_4. As seen from Figure 4e, MWCNT−PGMA did not show any response to the applied external magnetic field, whereas all MWCNT−Fe_3O_4 accumulated toward the external magnetic source, manifesting the strong magnetic performance of MWCNT−Fe_3O_4. Additionally, the magnetic properties of MWCNT−Fe_3O_4-2 complexes were directly measured by VSM. As seen from Figure 4f and its inset, the saturation magnetizations and coercivity of MWCNT−Fe_3O_4-2 were determined to be 16.5 emu g^{-1} and 75 Oe, respectively. All these results demonstrated that the deposited nanoparticles were ferromagnetic Fe_3O_4 nanoparticles, which were also consistent with the results of FT-IR and TGA characterizations. Therefore, MWCNT−Fe_3O_4 complexes were successfully prepared via PGMA-grafting and coprecipitation processes. The uniform distribution of Fe_3O_4 nanoparticles on the surface of MWCNT was attributed to the electrostatic repulsion between the positively charged nanoparticles as well as the impeding effect on the aggregation of nanoparticles by the introduction of TMAOH.

3.2. Observation of MWCNT−Fe_3O_4 Alignment. The possibility of the alignment of MWCNT−Fe_3O_4 complexes in the presence of an external magnetic field was investigated by changing factors including the intensity of the external magnetic field, loading content of Fe_3O_4 nanoparticles, and viscosity of dispersing medium. The effect of the intensity of the magnetic field on the alignment is shown in Figure 5. At the

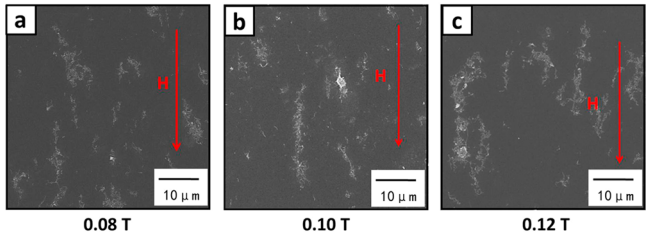

Figure 5. SEM images of MWCNT−Fe_3O_4-2 dispersed in deionized water in a magnetic field at intensities of (a) 0.08 T, (b) 0.10 T, and (c) 0.12 T.

three intensities of 0.08, 0.10, and 0.12 T, MWCNT−Fe_3O_4 complexes in deionized water showed responses to the applied magnetic field, in which, the resulting dipolar interactions reoriented the MWCNTs and favored the formation of chains of MWCNTs due to the presence of ferromagnetic Fe_3O_4 nanoparticles along MWCNTs. These chainlike structures were suggested to be a MWCNTs touching each other in a head-to-tail fashion, forming lines.[21,22] Noticeably, MWCNT−Fe_3O_4-2 was best aligned and parallel to the axis direction (i.e., north to south pole) of the magnetic field when the intensity of magnetic field was 0.10 T (Figure 5b), while it was only partially aligned in the other two situations (Figure 5a,c). It was well-known that the magnetic object normally tended to rotate under the effect of the magnetic moment derived from the magnetic field force, and it would finally reach the stable state when parallel to the axis direction of magnetic field. Thus, the

DOI: 10.1021/am507583r
ACS Appl. Mater. Interfaces 2015, 7, 3170−3179

force of magnetic field at the intensity of 0.08 T was thought not to be strong enough to make all of the MWCNT−Fe_3O_4 well-aligned along the axis direction of magnetic field. When the intensity of the magnetic field increased to 0.10 T, the magnetic field force was increased, which was beneficial to enhancing the alignment degree of MWCNT. However, at the higher intensity of 0.12 T, MWCNT−Fe_3O_4-2 was not more orderly aligned along the axis direction of the magnetic field as expected, but it tended to form clusters with irregular arrangement. It was proposed that too strong a magnetic field force applied on MWCNT might cause the movement of all of the MWCNT−Fe_3O_4 and result in a stack. Therefore, these observations revealed that the alignment state of MWCNT−Fe_3O_4 was sensitive to the intensity of magnetic field. The optimum alignment of MWCNT−Fe_3O_4 could be achieved when the intensity value of the magnetic field was in a proper range to balance the stretching state of MWCNT−Fe_3O_4.

MWCNT−Fe_3O_4 complexes containing various contents of Fe_3O_4 nanoparticles were then dispersed in deionized water and put in the magnetic field at an intensity of 0.10 T. As shown in Figure 6a,c, both MWCNT−Fe_3O_4-1 and MWCNT−Fe_3O_4-3 were partially aligned along the axis direction of the magnetic field, and some aggregated clusters were found at the same time. In contrast, MWCNT−Fe_3O_4-2 was well-aligned along the axis direction of the magnetic field (Figure 6b). The reason behind these phenomena was the difference in loading contents of Fe_3O_4 nanoparticles onto MWCNTs, since the value of the magnetic field force applied on MWCNT was directly proportional to the content of the magnetic component in the magnetic field with a fixed intensity; i.e., a higher content of Fe_3O_4 nanoparticles resulted in a higher magnetic field force. As aforementioned, the desirable alignment of MWCNT−Fe_3O_4 could be obtained only at the condition of applying the proper magnetic field force. MWCNT−Fe_3O_4-3, which contained 8 wt % content of Fe_3O_4 nanoparticles, was apparently not able to get enough magnetic field force to stretch, while MWCNT−Fe_3O_4-1 underwent so strong a magnetic field force as to cause aggregates because of its 33 wt % content of Fe_3O_4 nanoparticles. MWCNT−Fe_3O_4-2 with 26 wt % content of Fe_3O_4 nanoparticles was found to have the strongest ability to align in the magnetic field at an intensity of 0.10 T. Thus, the optimum alignment of MWCNT−Fe_3O_4 could be achieved in the magnetic field with a fixed intensity when the loading content of Fe_3O_4 nanoparticles onto MWCNT was in the proper range.

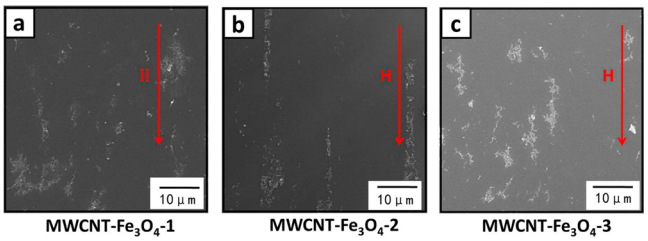

Figure 6. SEM images of (a) MWCNT−Fe_3O_4-1, (b) MWCNT−Fe_3O_4-2, and (c) MWCNT−Fe_3O_4-3 dispersed in deionized water in a magnetic field at an intensity of 0.10 T.

In addition to deionized water, two other dispersing media (isobutyl alcohol and ethylene glycol) were also used as dispersing media for MWCNT−Fe_3O_4 complexes. From Figure 7, it could be seen that MWCNT−Fe_3O_4-2 in both deionized water and isobutyl alcohol was mostly aligned along the axis direction of the magnetic field, while only a few of MWCNT−Fe_3O_4-2 were aligned along the axis direction of the magnetic field in ethylene glycol. Apparently, this phenomenon resulted from the viscosity difference of the used dispersing media, which were 1.0, 4.7, and 19.9 mPa·s at room temperature for deionized water, isobutyl alcohol, and ethylene glycol, respectively. Higher viscosity would generate stronger drag force to further hinder the movement of MWCNTs when they were stretched and rotated by the magnetic field force. Theoretically, dispersing medium with low viscosity would favor MWCNT−Fe_3O_4 being aligned along the axis direction of the magnetic field.

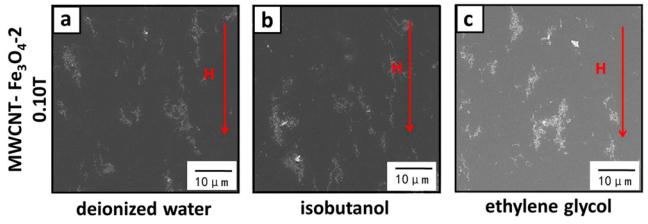

Figure 7. SEM images of MWCNT−Fe_3O_4-2 dispersed in (a) deionized water, (b) isobutyl alcohol, and (c) ethylene glycol in a magnetic field at an intensity of 0.10 T.

3.3. Numerical Characterization of MWCNT−Fe_3O_4 Alignment. To elucidate the effects of the intensity of the magnetic field, the loading content of Fe_3O_4 nanoparticles, and the viscosity of the dispersing medium on the alignment of MWCNT−Fe_3O_4 more clearly, it was necessary to quantitatively characterize the corresponding alignment state. Normally, the orientation tensor description was successfully established to characterize the orientation states of short fibers.[38] Since one-dimensional CNTs were similar to short fibers in geometry, the orientation tensor description could be used as an effective way to denote the alignment directions of MWCNT−Fe_3O_4 in the present study. Compared to the indirect characterizations of CNT directions, such as Raman spectroscopy[25] and polarized light diffraction,[39] the orientation tensor method showed the advantage of directly quantifying MWCNT−Fe_3O_4 alignment angles and detecting all the MWCNT−Fe_3O_4 appearing in the selected area.

The second moments of the probability distribution function, called orientation tensors, were applied and defined as eq 1:[38,40]

$$\langle \mathbf{m} \rangle = \langle w_i w_j \rangle = \oint w_i w_j \alpha(\mathbf{W})\, d\mathbf{W} \quad (1)$$

where $\mathbf{W}$ is the unit vector along the average direction of the CNT length. As shown in Figure 8, w_i and w_j are components of this vector along the coordinate directions. Herein, the orientation tensor description in the two-dimensional (2D) plane was adopted so that w_i and w_j were defined as eq 2 in the 2D plane[38]

$$w_1 = \sin\beta, \quad w_2 = \cos\beta \quad (2)$$

where β denotes the alignment angle for an individual MWCNT−Fe_3O_4. Noticeably, for calculating the components of orientation tensor $\langle \mathbf{m} \rangle$ in the selected area, the distribution direction of each MWCNT−Fe_3O_4 needed to be measured experimentally.

DOI: 10.1021/am507583r
ACS Appl. Mater. Interfaces 2015, 7, 3170−3179

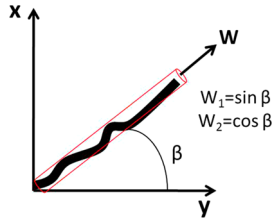

Figure 8. Definition of the direction of a single MWCNT by a unit vector **W** in the 2D plane. β is the orientation angle of a single MWCNT in the 2D plane.

The component m_{ij} in any area containing certain amounts (N) of MWCNTs was obtained using eq 3:[38,40]

$$m_{ij} = \frac{1}{N}\sum_{k=1}^{N} w_i^k w_j^k \tag{3}$$

As shown in Figure 9, vectors were marked in the optical microscope images in accordance to the length direction of each set of MWCNTs. The alignment angle of each set of MWCNT−Fe_3O_4 was measured with ImageJ software. The orientation tensor results at various conditions are shown in Figure 10. The ellipses are used to graphically describe the corresponding orientation state, and the related parameters for

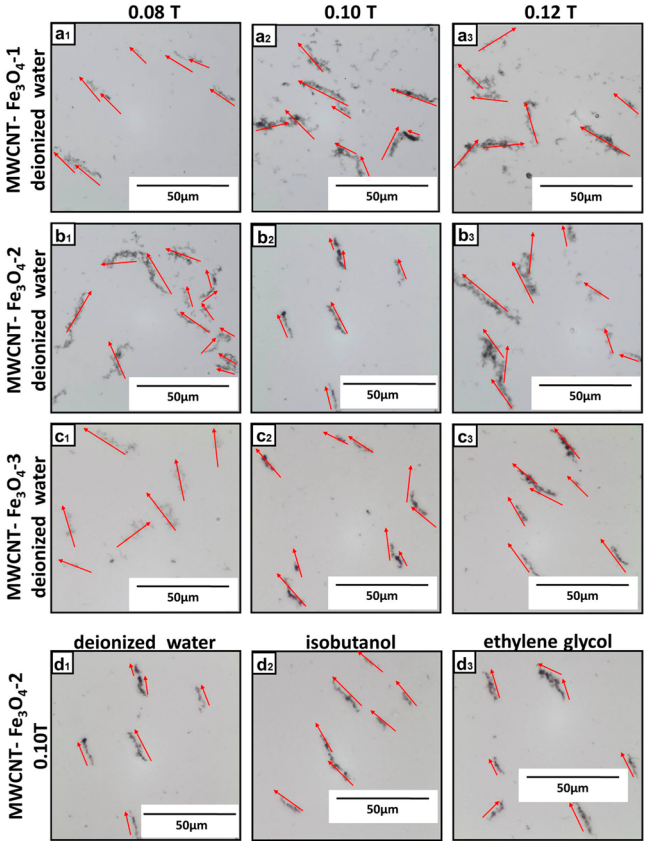

Figure 9. Optical images of (a_1−a_3) MWCNT−Fe_3O_4-1, (b_1−b_3) MWCNT−Fe_3O_4-2, and (c_1−c_3) MWCNT−Fe_3O_4-3 dispersed in deionized water in a magnetic field of various intensities, as well as optical images of MWCNT−Fe_3O_4-2 dispersed in (d_1) deionized water, (d_2) isobutyl alcohol, and (d_3) ethylene glycol in a magnetic field at an intensity of 0.10 T.

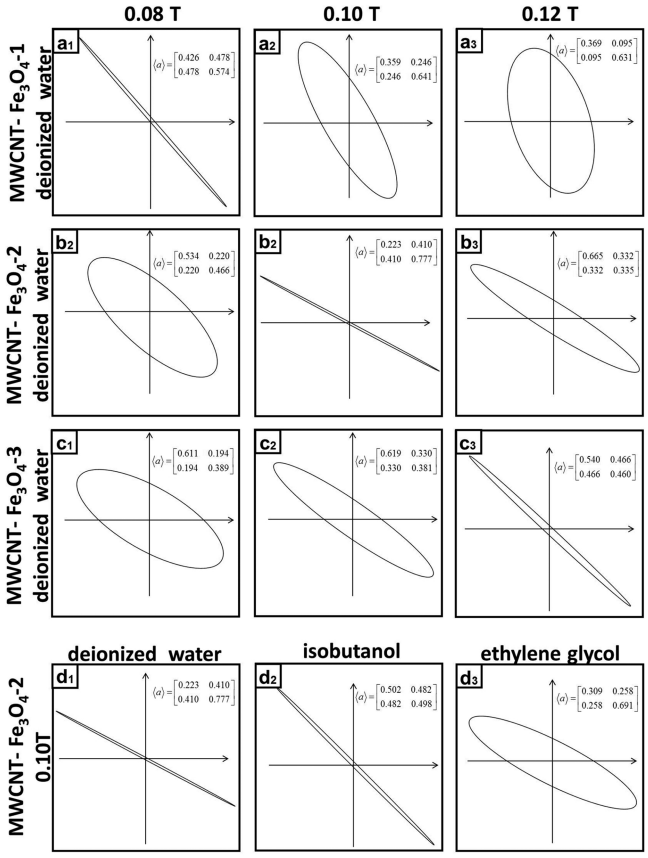

Figure 10. Second-order orientation tensors and ellipses of (a_1−a_3) MWCNT−Fe_3O_4-1, (b_1−b_3) MWCNT−Fe_3O_4-2, and (c_1−c_3) MWCNT−Fe_3O_4-3 dispersed in deionized water in a magnetic field of various intensities, as well as second-order orientation tensors and ellipses of MWCNT−Fe_3O_4-2 dispersed in (d_1) deionized water, (d_2) isobutyl alcohol, and (d_3) ethylene glycol in a magnetic field at an intensity of 0.10 T.

such ellipses were calculated by diagonalization from $\langle \mathbf{m} \rangle$ to the second-order orientation tensor $\langle \mathbf{m} \rangle^*$ based on eq 4:[40]

$$\mathbf{R}\langle \mathbf{m} \rangle \mathbf{R}^{\mathrm{T}} = \begin{bmatrix} \cos\alpha & \sin\alpha \\ -\sin\alpha & \cos\alpha \end{bmatrix} \begin{bmatrix} m_{11} & m_{12} \\ m_{21} & m_{22} \end{bmatrix} \begin{bmatrix} \cos\alpha & \sin\alpha \\ -\sin\alpha & \cos\alpha \end{bmatrix}^{\mathrm{T}}$$
$$= \begin{bmatrix} m_{11}^* & 0 \\ 0 & m_{22}^* \end{bmatrix}$$
$$= \langle \mathbf{m} \rangle^* \tag{4}$$

where m_{11}^* and m_{22}^*, respectively, denote the length of major and minor axes of the ellipse. α contained in the rotation matrix $\langle \mathbf{R} \rangle$ is the angle that the major axis is rotated anticlockwise from the horizon axis X. The calculated values for $\langle \mathbf{m} \rangle^*$ at various conditions are listed in Table 2. Thus, on the basis of these values, the ellipses were drawn as shown in Figure 10. The values of the major and minor axes for these ellipses characterized the orientation degree in the corresponding direction. Therefore, the major axes indicated the direction of preferential alignment of MWCNTs, and the preferential alignment degree (PAD) could be numerically calculated from eq 5:[38,40]

$$\mathrm{PAD} = \frac{m_{11}^* - m_{22}^*}{m_{11}^* + m_{22}^*} \tag{5}$$

DOI: 10.1021/am507583r
ACS Appl. Mater. Interfaces 2015, 7, 3170−3179

Table 2. Values of the Second-Order Orientation Tensor ⟨m⟩* and PAD at Various Conditions

sample	dispersing medium	magnetic field intensity (T)	major axes length (m_{11}^*)	minor axes length (m_{22}^*)	α in ⟨R⟩	PAD (%)
MWCNT− Fe_3O_4-1	deionized water	0.08	0.984	0.016	130.72	96.8
		0.10	0.783	0.217	119.99	56.6
		0.12	0.661	0.339	107.87	32.2
MWCNT− Fe_3O_4-2	deionized water	0.08	0.724	0.276	138.03	44.8
		0.10	0.995	0.005	152.00	98.9
		0.12	0.870	0.130	148.33	74.0
MWCNT− Fe_3O_4-3	deionized water	0.08	0.724	0.276	149.78	44.8
		0.10	0.851	0.149	144.87	70.2
		0.12	0.968	0.032	137.24	93.6
MWCNT− Fe_3O_4-2	deionized water	0.10	0.995	0.005	152.00	98.9
	isobutyl alcohol		0.982	0.018	135.17	96.4
	ethylene glycol		0.821	0.179	153.26	64.2

The obtained PAD values are also listed in Table 2. When MWCNT−Fe_3O_4 complexes were dispersed in deionized water, high PAD values (>90%) were found in three cases, i.e., MWCNT−Fe_3O_4-1/0.08 T, MWCNT−Fe_3O_4-2/0.10 T, and MWCNT−Fe_3O_4-3/0.12 T. It signified the formation of a highly aligned MWCNT−Fe_3O_4, namely, high alignment preference. In these cases, the ellipses in Figure 10a_1,b_2,c_3 demonstrate a subcircular geometry. PAD values in other cases were found to decrease, accompanied by the ellipses becoming less elongated in shape. When the loading content of Fe_3O_4 nanoparticles (MWCNT−Fe_3O_4-1) was high, the PAD values decreased as the intensity of the magnetic field increased. When the loading content of Fe_3O_4 nanoparticles (MWCNT−Fe_3O_4-3) was low, the highest alignment preference was obtained at an intensity of 0.12 T. These results revealed that the desirable alignment preference of MWCNT−Fe_3O_4 could be achieved by adjusting both the intensity of the magnetic field and the loading content of Fe_3O_4 nanoparticles to balance them. Therefore, MWCNT−Fe_3O_4-2 with 26 wt % content of Fe_3O_4 nanoparticles achieved the highest PAD value at an intensity of 0.10 T when dispersed in deionized water. However, a higher intensity of magnetic field was required to obtain a high alignment preference when the viscosity of the dispersing medium increased. As shown in Figure 10d_1−d_3 and Table 2, the alignment preference of MWCNT−Fe_3O_4-2 in ethylene glycol decreased when the intensity of the magnetic field remained 0.10 T.

With these approaches, the alignment mechanism of MWCNT−Fe_3O_4 was proposed and is illustrated in Figure 11. It was found that the intensity of the external magnetic field, loading content of Fe_3O_4 nanoparticles, and viscosity of dispersing medium were the determinant factors for the alignment state of MWCNT−Fe_3O_4. The applied magnetic field force on MWCNT−Fe_3O_4 was proportional to the intensity of the magnetic field and loading content of Fe_3O_4 nanoparticles, which obviously dominated the alignment degree of MWCNT−Fe_3O_4. With a low content of Fe_3O_4 nanoparticles, MWCNT−Fe_3O_4 was only partially stretched by the applied magnetic field force, when the suspension of MWCNT−Fe_3O_4 was placed in the external magnetic field at low intensity. As the intensity of the magnetic field increased and a balance between the magnetic field force and van der Waals force among MWCNT−Fe_3O_4 complexes was achieved, MWCNT−Fe_3O_4 could be well-aligned in chains and almost parallel to each other, just as found in the literature.[41] When the magnetic field force applied on MWCNT−Fe_3O_4 largely surpassed the van der Waals force among MWCNT−Fe_3O_4

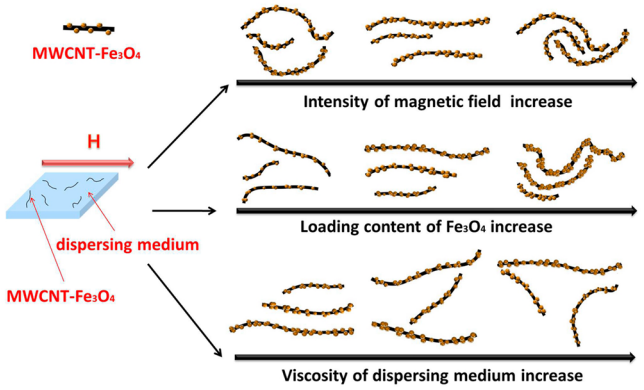

Figure 11. Schematic illustration for the alignment mechanism of MWCNT−Fe_3O_4 at various conditions.

complexes, MWCNT−Fe_3O_4 tended to accumulate together at the edge of magnetic field. In the case of MWCNT−Fe_3O_4 containing a high content of Fe_3O_4 nanoparticles, adversely, it might be disadvantageous to increase the intensity of the magnetic field with the intent to enhance the alignment preference. When the applied magnetic field force was kept constant, the alignment state of MWCNT−Fe_3O_4 would be dominated by the viscosity of the dispersing medium. If the medium possessed a high viscosity, it was highly possible that the magnetic field force was not strong enough to overcome the medium-derived drag and friction forces on MWCNT−Fe_3O_4. Therefore, the microscale movement and rotation of MWCNT−Fe_3O_4 was distinctively limited; in other words, MWCNT−Fe_3O_4 could not be stretched to align along the direction of the magnetic field. Only if the viscosity of the dispersing medium was in a relatively low range could the optimum alignment of MWCNT−Fe_3O_4 be achieved.

3.4. Evaluation of Mechanical Properties of Epoxy Composites with Aligned MWCNT−Fe_3O_4. With the aim of evaluating the advantages of aligned MWCNT−Fe_3O_4 in the application of reinforcement, MWCNT−Fe_3O_4-1 was selected for the preparation of epoxy-based composites, and their mechanical properties were tested. The reason for selecting MWCNT−Fe_3O_4-1 was that it was envisioned to achieve better alignment in viscous epoxy resin because of its higher content of Fe_3O_4 nanoparticles. Figure 12 shows the tensile and flexural properties of pristine epoxy and epoxy composites with 0.5 wt % of MWCNT−Fe_3O_4-1 without and with the application of an external magnetic field. In comparison with the data of pristine epoxy, epoxy composites with MWCNT−Fe_3O_4-1, prepared

DOI: 10.1021/am507583r
ACS Appl. Mater. Interfaces 2015, 7, 3170−3179

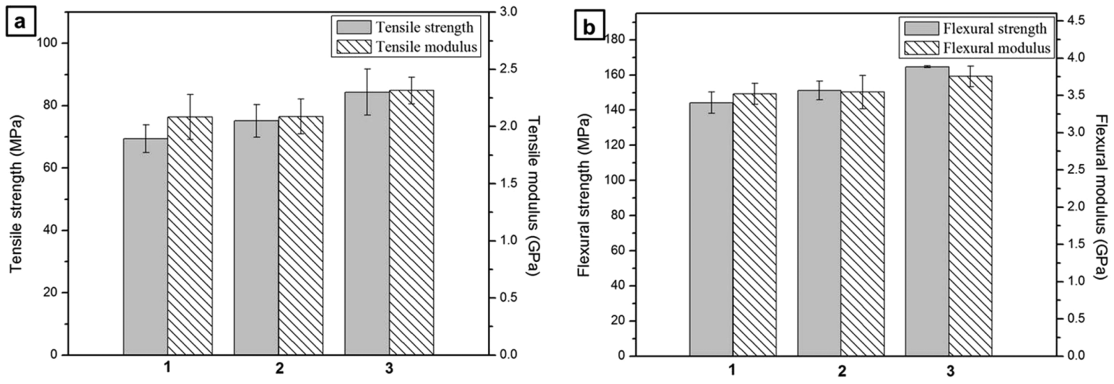

Figure 12. (a) Tensile and (b) flexural properties of (1) pristine epoxy and epoxy composites with 0.5 wt % of MWCNT−Fe_3O_4-1 prepared (2) without and (3) with the application of an external magnetic field.

with or without an external magnetic field, apparently demonstrated higher tensile and flexural properties, showing the reinforcing effect of MWCNT. With the addition of 0.5 wt % of MWCNT−Fe_3O_4-1 into the epoxy in the absence of a magnetic field, the tensile strength and modulus of the resulting composite reached 75.1 ± 5.2 MPa and 2.1 ± 0.1 GPa, respectively. The application of a magnetic field could further enhance the values by 12.3 and 10.9%, respectively. A similar trend was detected in flexural properties of epoxy composites; i.e., the flexural strength and modulus were enhanced by 8.9 and 6.1% when the external magnetic field was applied in preparing epoxy composites with MWCNT−Fe_3O_4. Similar results were also reported in the literature.[42−44] These enhancements were attributed to the directional alignment of MWCNT−Fe_3O_4-1 in the epoxy matrix along the length direction of specimens, since the magnetic field was set parallel to the length direction. It was suggested that the aligned CNTs were able to bear more loads and subsequently enhance the effective stress transfer in the composites by taking full advantage of the superior mechanical strength and modulus of CNTs themselves.[43,45] This finding provided the practical possibility of applying magnetic CNTs as a reinforcement for resins, in which the CNTs could be effectively aligned by applying the proper magnetic field to achieve high-performance composites.

4. CONCLUSIONS

Coprecipitation of surface-grafted MWCNT with iron salts under basic condition was proven to be an efficient and controllable way to prepare MWCNT−Fe_3O_4 complexes. The loaded Fe_3O_4 nanoparticles distributed uniformly on the surface of MWCNTs, and their ferromagnetism made MWCNT−Fe_3O_4 complexes respond to the magnetic field force generated by an external magnetic field. In obtaining desirable alignment of MWCNT−Fe_3O_4 complexes along the axis direction (i.e., north to south pole) of a magnetic field, a balance between the magnetic field force and the resistance in stretching and rotating was the key consideration. In addition to the viscosity of the dispersing medium, the loading content of Fe_3O_4 nanoparticles and the intensity of the external magnetic field also demonstrated interdependency in regulating the balance. Epoxy/MWCNT−Fe_3O_4 composites prepared under proper parameters displayed a prominent reinforcing effect when MWCNT−Fe_3O_4 complexes were magnetically aligned effectively in the resin matrix. The proposed quantitative characterization with an orientation tensor description was quite helpful in illustrating the preferential alignment degree of MWCNTs, which provided a feasible approach to modulate the distribution state and to exploit the intrinsic high performance of MWCNTs in practical applications.

AUTHOR INFORMATION

Corresponding Author

*Tel/Fax: +86-10-6441-2884. E-mail: caiqing@mail.buct.edu.cn.

Notes

The authors declare no competing financial interest.

ACKNOWLEDGMENTS

The authors are very pleased to acknowledge financial support from the National Natural Science Foundation of China (Grant No. U1362205), Natural Science Foundation of Jiangsu Province (Grant No. BK20140271), National High Technology Research and Development Program of China (Grant No. 2012AA03A203), Beijing Youth Talent Plan (Grant No. YETP0492) and 2014 Open Project of State Key Laboratory of Organic−Inorganic Composites.

REFERENCES

(1) Iijima, S.; Ajayan, P. M.; Ichihashi, T. Growth Model for Carbon Nanotubes. *Phys. Rev. Lett.* **1992**, *69*, 3100−3103.

(2) Sarka, S.; Zou, J. H.; Li, J. H.; Xu, C. Y.; An, L.; Zhai, L. Polymer-Derived Ceramic Composite Fibers with Aligned Pristine Multiwalled Carbon Nanotubes. *ACS Appl. Mater. Interfaces* **2010**, *2*, 1150−1156.

(3) Barman, S. N.; Lemieux, M. C.; Baek, J.; Rivera, R.; Bao, Z. N. Effects of Dispersion Conditions of Single-Walled Carbon Nanotubes on the Electrical Characteristics of Thin Film Network Transistors. *ACS Appl. Mater. Interfaces* **2010**, *2*, 2672−2678.

(4) Thea, I. S.; Graeme, S.; Dominik, E.; Krzysztof, K. K.; Burstein, G. T.; Alan, H. W. The Production of Aligned MWCNT/Polypyrrole Composite Films. *Carbon* **2013**, *60*, 229−235.

(5) Lee, J. H.; Kim, N. R.; Kim, B. J.; Joo, Y. C. Improved Mechanical Performance of Solution-Processed MWCNT/Ag Nanoparticle Composite Flms with Oxygen-Pressure-Controlled Annealing. *Carbon* **2012**, *50*, 98−106.

(6) Chen, Z. Q.; Dai, X. J.; Magniez, K.; Lamb, P. R.; Leal, D. R.; Fox, B. L. Improving the Mechanical Properties of Epoxy Using Multiwalled Carbon Nanotubes Functionalized by a Novel Plasma Treatment. *Composites, Part A* **2013**, *45*, 145−152.

(7) Jeong, W.; Kessler, M. R. Toughness Enhancement in ROMP Functionalized Carbon Nanotube/Polydicyclopentadiene Composites. *Chem. Mater.* **2008**, *20*, 7060−7068.

DOI: 10.1021/am507583r
ACS Appl. Mater. Interfaces 2015, 7, 3170−3179

(8) Lubineau, G.; Rahaman, A. A Review of Strategies for Improving the Degradation Properties of Laminated Continuous-Fiber/Epoxy Composites with Carbon Based Nanoreinforcements. *Carbon* **2012**, *50*, 2377−2395.
(9) Allen, R.; Fuller, G. G.; Bao, Z. N. Aligned SWNT Films from Low-Yield Stress Gels and Their Transparent Electrode Performance. *ACS Appl. Mater. Interfaces* **2013**, *5*, 7244−7252.
(10) Vigolo, B.; Pénicaud, A.; Coulon, C.; Sauder, C.; Pailler, R.; Journet, C. Macroscopic Fibers and Ribbons of Oriented Carbon Nanotubes. *Science* **2000**, *290*, 1331−1334.
(11) Kimura, T.; Ago, H.; Tobita, M.; Ohshima, S. Polymer Composites of Carbon Nanotubes Aligned by a Magnetic Field. *Adv. Mater.* **2002**, *14*, 1380−1383.
(12) Steinert, B. W.; Dean, D. R. Magnetic Field Alignment and Electrical Properties of Solution Cast PET−Carbon Nanotube Composite Films. *Polymer* **2009**, *50*, 898−904.
(13) Sen, R.; Zhao, B.; Perea, D.; Itkis, M. E.; Hu, H.; Love, J. Preparation of Single-Walled Carbon Nanotube Reinforced Polystyrene and Polyurethane Nanofibers and Membranes by Electrospinning. *Nano Lett.* **2004**, *4*, 459−464.
(14) Shinji, I.; Hidetoshi, M.; Yuichi, K.; Kazuma, T.; Mie, M.; Akihiko, T.; Krzysztof, K.; Alan, W. Top-Down Process Based on Electrospinning, Twisting, and Heating for Producing One-Dimensional Carbon Nanotube Assembly. *ACS Appl. Mater. Interfaces* **2011**, *3*, 469−475.
(15) Noe, J. M.; Silvia, G.; Claudio, C.; Victoria, B.; Roberto, J. C.; Gerardo, H. R. One-Step Chemical Vapor Deposition Synthesis of Magnetic CNT−Hercynite ($FeAl_2O_4$) Hybrids with Good Aqueous Colloidal Stability. *Carbon* **2013**, *61*, 515−524.
(16) Emilio, M. S.; Nestor, P. L.; Rodolfo, L. J.; Gladis, L. D.; Beatriz, R. E.; Adalberto, Z. Synthesis, Characterization and Magnetic Properties of Co@Au Core-Shell Nanoparticles Encapsulated by Nitrogen-Doped Multiwall Carbon Nanotubes. *Carbon* **2014**, *77*, 722−737.
(17) Korneva, G.; Ye, H.; Gogotsi, Y.; Halverson, D.; Friedman, G.; Bradley, J. C. Carbon Nanotubes Loaded with Magnetic Particles. *Nano Lett.* **2005**, *5*, 879−884.
(18) Gao, C.; Li, W.; Morimoto, H.; Nagaoka, Y.; Maekawa, T. Magnetic Carbon Nanotubes: Synthesis by Electrostatic Self-Assembly Approach and Application in Biomanipulations. *J. Phys. Chem. B* **2006**, *110*, 7213−7220.
(19) Lin, T. W.; Salzmann, C. G.; Shao, L. D.; Yu, C. H.; Green, M. L.; Tsang, S. C. Polyethylene Glycol Grafting and Attachment of Encapsulated Magnetic Iron Oxide Silica Nanoparticles onto Chlorosilanized Single-Wall Carbon Nanotubes. *Carbon* **2009**, *47*, 1415−1420.
(20) Cao, M. S.; Yang, J.; Song, W. L.; Zhang, D. Q.; Wen, B.; Jin, H. B. Ferroferric Oxide/Multiwalled Carbon Nanotube vs Polyaniline/Ferroferric Oxide/Multiwalled Carbon Nanotube Multiheterostructures for Highly Effective Microwave Absorption. *ACS Appl. Mater. Interfaces* **2012**, *12*, 6949−6956.
(21) Kim, I. T.; Tannenbaum, A.; Tannenbaum, R. Anisotropic Conductivity of Magnetic Carbon Nanotubes Embedded in Epoxy Matrices. *Carbon* **2011**, *49*, 54−61.
(22) Correa-Duarte, M. A.; Grzelczak, M.; Salgueiriño-Maceira, V.; Giersig, M.; Liz-marzan, L. M.; Farle, M. Alignment of Carbon Nanotubes under Low Magnetic Fields through Attachment of Magnetic Nanoparticles. *J. Phys. Chem. B* **2005**, *109*, 19060−19063.
(23) Ma, P. C.; Siddiqui, N. A.; Marom, G.; Kim, J. K. Dispersion and Functionalization of Carbon Nanotubes for Polymer-Based Nanocomposites: A Review. *Composites, Part A* **2010**, *41*, 1345−1367.
(24) Jia, X.; Li, G.; Liu, B.; Luo, Y.; Yang, G.; Yang, X. Multiscale Reinforcement and Interfacial Strengthening on Epoxy-Based Composites by Silica Nanoparticle-Multiwalled Carbon Nanotube Complex. *Composites, Part A* **2013**, *48*, 101−109.
(25) Ji, J.; Sui, G.; Yu, Y.; Liu, Y.; Lin, Y.; Du, Z. Significant Improvement of Mechanical Properties Observed in Highly Aligned Carbon-Nanotube-Reinforced Nanofibers. *J. Phys. Chem. C* **2009**, *113*, 4779−4785.
(26) Sui, G.; Xue, S. S.; Bi, H. T.; Yang, X. P. Desirable Electrical and Mechanical Properties of Continuous Hybrid Nano-Scale Carbon Fibers Containing Highly Aligned Multi-Walled Carbon Nanotubes. *Carbon* **2013**, *64*, 72−83.
(27) Qu, S.; Wang, J.; Kong, J.; Yang, P.; Chen, G. Magnetic Loading of Carbon Nanotube/Nano-Fe_3O_4 Composite for Electrochemical Sensing. *Talanta* **2007**, *71*, 1096−1102.
(28) Chen, W. M.; Yu, Y. H.; Li, P.; Wang, C. Z.; Zhou, T. Y.; Yang, X. P. Effect of New Epoxy Matrix for T800 Carbon Fiber/Epoxy Filament Wound Composites. *Compos. Sci. Technol.* **2007**, *67*, 2261−2270.
(29) Zhu, A. P.; Shi, Z. H.; Cai, A. Y.; Zhao, F.; Liao, T. Q. Synthesis of Core-Shell PMMA−SiO_2 Nanoparticles with Suspension−Dispersion−Polymerization in an Aqueous System and Its Effect on Mechanical Properties of PVC Composites. *Polym. Test.* **2008**, *27*, 540−547.
(30) Shi, D.; Cheng, J. P.; Liu, F.; Zhang, X. B. Controlling the Size and Size Distribution of Magnetite Nanoparticles on Carbon Nanotubes. *J. Alloys Compd.* **2010**, *502*, 365−370.
(31) Gao, C.; Vo, C. D.; Jin, Y. Z.; Li, W.; Armes, S. P. Multihydroxy Polymer-Functionalized Carbon Nanotubes: Synthesis, Derivatization, and Metal Loading. *Macromolecules* **2005**, *38*, 8634−8648.
(32) Li, W.; Gao, C.; Qian, H.; Ren, J.; Yan, D. Multiamino-Functionalized Carbon Nanotubes and Their Applications in Loading Quantum Dots and Magnetic Nanoparticles. *J. Mater. Chem.* **2006**, *16*, 1852−1859.
(33) Zhang, W. D.; Xiao, H. M.; Zhu, L. P.; Fu, S. H.; Wan, M. X. Facile One-Step Synthesis of Electromagnetic Functionalized Polypyrrole/Fe_3O_4 Nanotubes via a Self-Assembly Process. *J. Polym. Sci., Part A: Polym. Chem.* **2010**, *48*, 320−326.
(34) Sophie, L.; Delphine, F.; Marc, P.; Alain, R.; Caroline, R.; Luce, V. E. Magnetic Iron Oxide Nanoparticles: Synthesis, Stabilization, Vectorization, Physicochemical Characterizations, and Biological Applications. *Chem. Rev.* **2008**, *108*, 2064−2110.
(35) Pramanik, S.; Konwarh, R.; Deka, R. C.; Aidew, L.; barua, N.; Buragohain, A. K. Microwave-Assisted Poly(glycidyl methacrylate)-Functionalized Multiwall Carbon Nanotubes with a 'Tendrillar' Nanofibrous Polyaniline Wrapping and Their Interaction at Bio-Interface. *Carbon* **2013**, *55*, 34−43.
(36) Wang, C.; Wei, Y. J.; Jiang, H. Y.; Sun, S.H. Tug-of-War in Nanoparticles: Competitive Growth of Au on Au-Fe_3O_4 Nanoparticles. *Nano Lett.* **2009**, *9*, 4544−4547.
(37) Dong, L. X.; Tao, X. Y.; Li, Z.; Zhang, L.; Nelson, B. J. Nanorobotic Spot Welding: Controlled Metal Deposition with Attogram Precision from Copper-Filled Carbon Nanotubes. *Nano Lett.* **2007**, *7*, 58−63.
(38) Fan, Z.; Advani, S. G. Characterization of Orientation State of Carbon Nanotubes in Shear Flow. *Polymer* **2005**, *46*, 5232−5240.
(39) Hobbie, E. K.; Wang, H.; Kim, H.; Han, C. C.; Grulke, E. A.; Obrzut, J. Optical Measurements of Structure and Orientation in Sheared Carbon-Nanotube Suspensions. *Rev. Sci. Instrum.* **2003**, *74*, 1244−1250.
(40) Yao, S. H.; Yuan, J. K.; Zhou, T.; Dang, Z. M.; Bai, J. Stretch-Modulated Carbon Nanotube Alignment in Ferroelectric Polymer Composites: Characterization of the Orientation State and Its Influence on the Dielectric Properties. *J. Phys. Chem. C* **2011**, *115*, 20011−20017.
(41) Horton, M.; Hong, H.; Li, C.; Shi, B.; Peterson, G. P.; Jin, S. Magnetic Alignment of Ni-Coated Single Wall Carbon Nanotubes in Heat Transfer Nanofluids. *J. Appl. Phys.* **2010**, *107*, 104320/1−4.
(42) Abdalla, M.; Dean, D.; Theodore, M.; Fielding, J.; Nyairo, E.; Price, G. Magnetically Processed Carbon Nanotube/Epoxy Nanocomposites: Morphology, Thermal and Mechanical Properties. *Polymer* **2010**, *51*, 1614−1620.
(43) Goh, P. S.; Ismail, A. F.; Ng, B. C. Directional Alignment of Carbon Nanotubes in Polymer Matrices: Contemporary Approaches and Future Advances. *Composites, Part A* **2014**, *56*, 103−126.

DOI: 10.1021/am507583r
ACS Appl. Mater. Interfaces 2015, 7, 3170−3179

(44) Camponeschi, E.; Vance, R.; Al-Haik, M.; Garmestani, H.; Tannenbaum, R. Properties of Carbon Nanotube−Polymer Composites Aligned in a Magnetic Field. *Carbon* **2007**, *45*, 2037−2046.
(45) Wang, Q.; Dai, J. F.; Li, W. X.; Wei, Z. Q.; Jiang, J. L. The Effects of CNT Alignment on Electrical Conductivity and Mechanical Properties of SWNT/Epoxy Nanocomposites. *Compos. Sci. Technol.* **2008**, *68*, 1644−1648.

DOI: 10.1021/am507583r
ACS Appl. Mater. Interfaces 2015, 7, 3170−3179